6.6 AEROSOL INFLUENCES ON TORNADO GENESIS

David G. Lerach*, Brian J. Gaudet[1], and William R. Cotton
Colorado State University, Fort Collins, Colorado
[1]The Pennsylvania State University, University Park, Pennsylvania

1. Introduction

Aerosols, both natural and anthropogenic, impact hydrometeor formation and cloud and precipitation processes by acting as cloud condensation nuclei (CCN) and giant CCN (GCCN). Increasing CCN concentrations tends to inhibit the warm-rain process while increasing GCCN concentrations generally enhances them (Hobbs et al. 1970; Rosenfeld et al. 2002; Eagan et al. 1974; Braham et al. 1981; Kaufman and Nakajima 1993; Borys et al. 1998; Rosenfeld 1999, 2000). Seifert and Beheng (2006) showed that higher CCN concentrations in simulated multicell storms led to more supercooled water aloft, yielding stronger updrafts. Likewise, van den Heever et al. (2006) performed numerical simulations of ordinary convection, finding that higher CCN concentrations initially enhanced the upward transport of supercooled cloud droplets and associated latent heating and higher GCCN concentrations enhanced mature updraft strength through rapid glaciation. Being that hailstone growth principally occurs in the updraft where there is a close match between updraft velocities and the fall velocities of the stones (Foote 1984), enhanced aerosol concentrations acting as CCN and GCCN could yield production of larger hail in convective storms. While no studies have yet investigated possible aerosol effects on supercell thunderstorms, Weisman and Bluestein (1985) were among the first to suggest the importance of microphysical parameters to supercell thunderstorm dynamics. van den Heever and Cotton (2004) and Gilmore et al. (2004) addressed possible microphysical effects, finding that larger raindrop and hail diameters reduced evaporative cooling and melting rates, producing weaker low-level downdrafts and weaker, shallower cold pools. This suggests a possible link between aerosols and supercell tornadogenesis.

Fig. 1 depicts the structure of a tornadic supercell as described by Lemon and Doswell (1979). The main components include the forward flank downdraft (FFD), updraft (UP), rear flank downdraft (RFD), and gust front. While the precise mechanisms of supercell tornadogenesis remain unknown, multiple studies suggest that these tornadoes are often linked to the RFD, which can transport vertical vorticity to the surface, baroclinically generate horizontal vorticity, and enhance convergence along gust fronts beneath the updraft (Burgess et al. 1977; Davies-Jones 1982a,b; Davies-Jones and Brooks 1993; Walko 1993; Brooks et al. 1994; Wicker and Wilhelmson 1995; Trapp and Fiedler 1995; Markowski 2002).

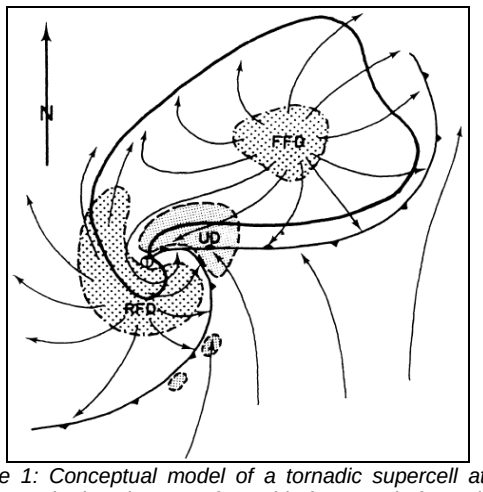

Figure 1: Conceptual model of a tornadic supercell at the surface. The location most favorable for tornado formation is marked by an encircled T. [From Lemon and Doswell (1979).]

Ludlam (1963) first argued that tornadogenesis is more likely to occur when the temperature deficit within the RFD is small relative to the environment. The theory was later supported by observations (Lemon 1974; Nelson 1977; Brandes 1978) and idealized numerical simulations (Eskridge and Das 1976; Davies-Jones 2000b; Leslie and Smith 1978). Observational and numerical modeling studies by Markowski et al. (2002, 2003), utilizing VORTEX data, found that air parcels within RFDs tended to be less negatively buoyant (warmer) in tornadic vs. nontornadic supercells. Tornadic vortices increased in intensity and longevity as downdraft parcel buoyancy

* Corresponding author address: David G. Lerach, Colorado State University, Dept. of Atmospheric Science, Fort Collins, CO 80523; email: dlerach@atmos.colostate.edu

increased, because colder parcels were more resistant to lifting. Snook and Xue (2008) extended the work of van den Heever and Cotton (2004) and Gilmore et al. (2004) to tornadogenesis, verifying that larger raindrops and hailstones yielded warmer cold pools via reduced evaporative cooling. In addition, the larger hydrometeors, with greater terminal fallspeeds, were not advected as far from the updraft before falling to the ground, reducing the areal coverage of precipitation. This positioned the gust front closer to the storm center, permitting vertically-oriented updrafts and vertical alignment of low- and mid-level vertical vorticity. This in turn increased the dynamic suction effect by the mesocyclone (Rotunno and Klemp 1982) and associated low-level vertical stretching, thereby increasing the potential for tornadogenesis.

The goal of this study is to investigate possible aerosol indirect microphysical influences on supercell tornadogenesis. Two numerical simulations of an idealized supercell thunderstorm are performed, differing only in initial background aerosol concentrations, representing "clean" and aerosol-polluted environments, respectively. The simulations are compared to assess which is more favorable for tornadogenesis. Note that the work presented herein has been published in Geophysical Research Letters (Lerach et al. 2008).

2. Model setup

This study utilized the Regional Atmospheric Modeling System (RAMS; Pielke et al. 1992) version 4.3.0 (Cotton et al. 2003) in a Cartesian coordinate domain. Three two-way interactive nested model grids (Clark and Farley 1984) were used with horizontal grid spacing of 1000, 333.33, and 111.11 m respectively. The outer-most grid (Grid 1), used for generating convection, had horizontal dimensions of 149x149 km. Grid 2, centered over Grid 1 coordinates (49 km, 29 km), had dimensions of 60.33x60.33 km and was used to simulate the scale of the supercell environment. Grid 3 was centered over Grid 2 coordinates (4.67 km, 4.67 km) and had horizontal dimensions of 38.44x21.78 km. This inner grid was used to assess the evolution of the mesocyclone and any tornadic vortices. This study defined a simulated tornado as a low-level vortex that met the following criteria adapted from Wicker and Wilhelmson (1995): (i) The vortex forms in conjunction with a supercell mesocyclone (ii) The vortex is characterized by highly convergent swirling winds affecting a relatively narrow path, and (iii) The near-surface winds exceed minimum EF-1 intensity (40 m s^{-1}).

A bin-emulating, two-moment bulk microphysics scheme (Saleeby and Cotton 2004) was utilized in these simulations, which included a microphysical category of large cloud droplets with diameters from 40 to 80 μm (cloud2) to better represent the frequently bimodal distribution of cloud droplet spectra. The scheme explicitly predicted mixing ratios and number concentrations of pristine ice, snow, aggregates, graupel, hail, cloud and cloud2 droplets, and rain. Nucleation by CCN, GCCN, and ice nuclei (IN) were explicitly considered. CCN (GCCN) directly nucleated to form cloud (cloud2) droplets. The model excluded the effects of terrain, surface fluxes, surface drag, radiation, and friction due to the time scales involved and the desire to simplify the experiment. Convection was explicitly resolved on all grids. Surface vegetation was assumed to be composed of crop/mixed farming, and the soil type was prescribed as sandy clay loam.

The initial sounding utilized (Fig. 2a-b) was one found to generate storm-splitting and supercells (Grasso 2000; van den Heever and Cotton 2004; Gaudet and Cotton 2006), of which this study focused on the right-mover. The initial vertical wind profile (Fig. 2e) was also adapted from that used in these previous studies. Convection was initiated by introducing a "warm, moist bubble" (10x10x1.5 km, 2 K thermal perturbation, 20% moisture perturbation) at the surface. The model aerosol species were set initially horizontally-homogeneous with prescribed vertical profiles of CCN, GCCN, and IN concentrations. In one simulation, initial background aerosol concentration profiles were set for a relatively "clean" continental environment (CLN). In the other, concentrations

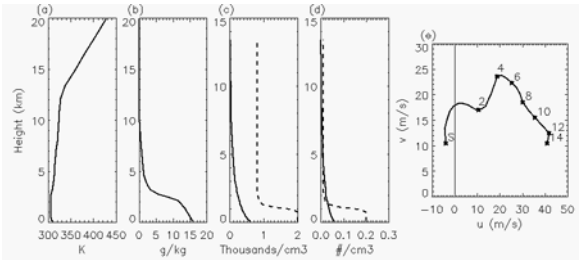

Figure 2: Initial profiles of (a) potential temperature, (b) mixing ratio, (c) CCN and (d) GCCN concentrations, and (e) Initial horizontal winds depicted as a hodograph (heights in km). In Fig 2c-d, CLN profiles are solid and POL profiles are dashed.

were increased to act as an aerosol-polluted environment (POL) due to dust or pollutants. CCN (GCCN) concentrations near the surface were set to 600 (0.06) cm^{-3} and 2000 (0.2) cm^{-3} for the CLN and POL simulations, respectively (Fig. 2c-d), based on CRYSTAL-FACE measurements (van den Heever et al. 2006). While IN concentrations are thought to be important to convective processes, their effects will be addressed in future studies. Here, the initial IN profile was held fixed between simulations. Simulations lasted two hours. Grid 2 was spawned at 60 min. Grid 3 was spawned at 85 min.

3. Results

a. Precipitation characteristics

Fig. 3 displays the time evolution of Grid 2 precipitation rate for both simulations. Updrafts (downdrafts) greater than 20 (5) m s^{-1} and at 2 km are overlaid. For simplicity the positive "y," negative "y," positive "x," and negative "x" directions will be referred to as north, south, east, and west, respectively. The simulated supercell storm initially evolves similarly between the CLN and POL cases. By 80 min, a pronounced hook-shaped structure has formed on the southern end of each storm that wraps cyclonically around the main updraft, associated with the RFD. Precipitation rates greater than 10 mm hr^{-1} generally lie within downdrafts greater than 5 m s^{-1}. The POL hook is more defined. However, the CLN supercell shows the strongest precipitation rates, with values greater than 100 mm hr^{-1} in the RFD and FFD. While precipitation rates greater than 100 mm hr^{-1} exist toward the rear of the POL RFD, maximum values in the FFD only reach 70 mm hr^{-1}. The hook-like structure is less defined at 90 min in both storms, though that of the POL supercell is more pronounced. Precipitation intensity evolves differently between the two storms after this time. The POL storm exhibits a distinct maximum in precipitation rate in the RFD just behind the main updraft. Precipitation rates are strengthening in the core of the CLN FFD but weakening within the dissipating RFD. The CLN FFD still contains significantly heavier precipitation rates than the POL case. At 100 min, the POL supercell maintains a well-defined RFD whereas the CLN RFD has essentially dissipated, leaving only a large FFD containing heavy rain with precipitation rates greater than 200 mm hr^{-1}. As the CLN updraft continues to

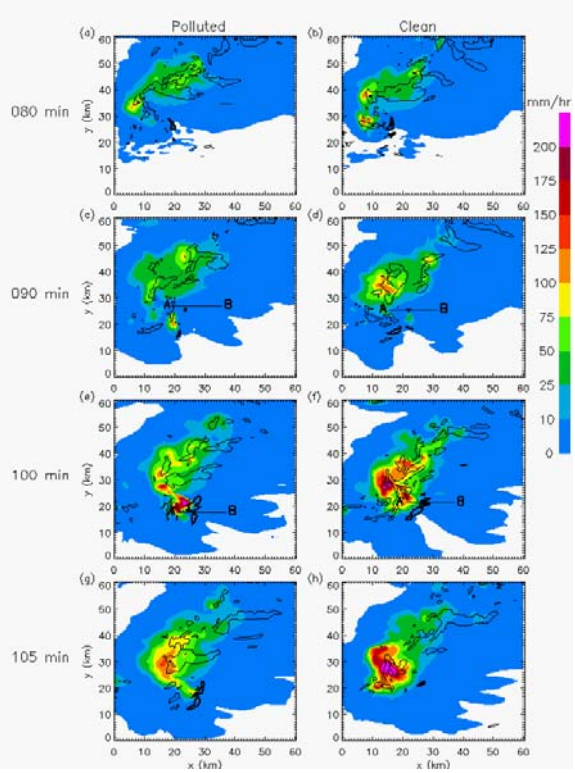

Figure 3: POL (left) and CLN (right) surface precipitation rate on Grid 2 overlaid with vertical velocity at 2 km: updrafts greater than 20 m s^{-1} (thick) and downdrafts greater than 5 m s^{-1} (thin). All x-y axis labels are grid-relative. [from Lerach et al. (2008).]

move ahead of the rest of the system, the POL updraft remains adjacent to the precipitation-filled RFD, now showing precipitation rates greater than 200 mm hr^{-1}. The POL case exhibits maximum precipitation rates in the southern portion of the RFD while the CLN case continues to show maximum rates further to the north. At 105 min, the POL case maintains a well-defined hook and a large region of updrafts greater than 20 m s^{-1} at 2 km. The POL RFD weakens as the storm's FFD produces most of the precipitation, with maximum precipitation rates near 150 mm hr^{-1}. The CLN supercell continues to dissipate, showing a single core of FFD precipitation and only remnants of a low-level updraft. The CLN case continues to produce the highest precipitation rates (> 200 mm hr^{-1}).

The POL simulation produces a steadier, longer-lived storm while the CLN simulation produces heavier rainfall. At 120 min, the pattern of total accumulated precipitation on Grid 2 (Fig. 4) in the POL case exhibits two distinct precipitation maxima greater than 50 mm associated with the storm's RFD and FFD. That of the CLN case shows only a single

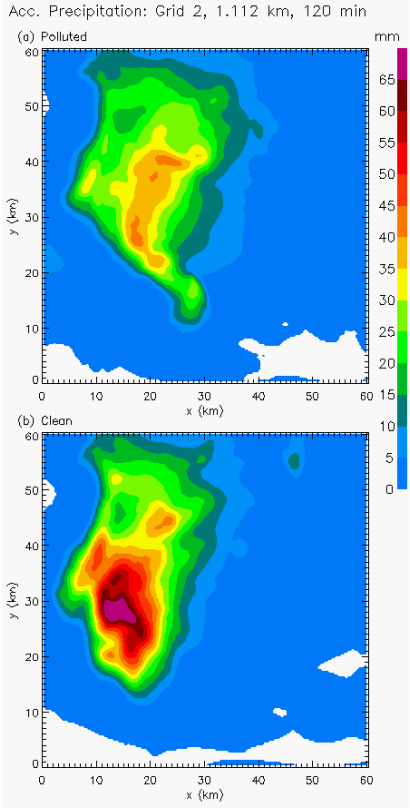

Figure 4: (a) POL and (b) CLN accumulated precipitation on Grid 2 at 120 min.

maximum greater than 65 mm, associated with the FFD. Notice that the FFD in the CLN simulation strengthens near 90min, overtaking the RFD (Fig. 3d).

b. Tornadogenesis on Grid 3

At 100 min the POL supercell produces a tornado-like vortex of EF-1 intensity, unlike the CLN supercell. Fig. 5 displays near-surface (24 m) pressure, vertical vorticity, horizontal winds, and potential temperature on Grid 3 for both simulations at 100 min over the POL low-level mesocyclone. The POL case shows the distinct formation of a strong low-pressure center of 989 mb associated with the tornado. Pressure increases rapidly north and south of the low, signifying the RFD- and FFD-based gust fronts. The CLN simulation attempts to create a similar pressure pattern. However, by 100 min the pressure center has weakened, leaving only a single line of relatively high pressure (> 995 mb) associated with a single gust front. The POL supercell produces a well-defined positive vertical vorticity center and cyclonic winds, associated with the tornadic vortex. An 'S'-shaped pattern in the vorticity field signifies the

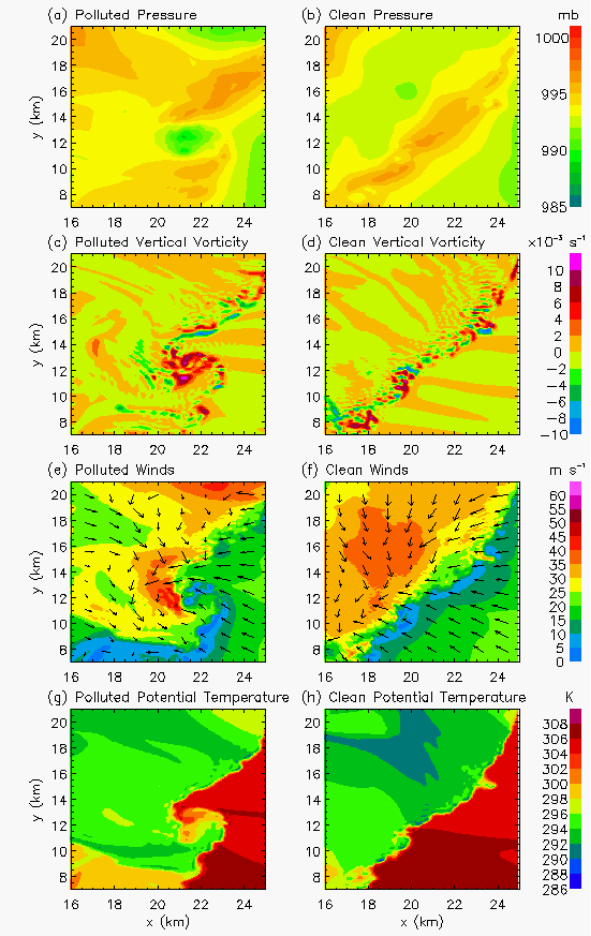

Figure 5: Grid 3 near-surface (24 m) pressure, vertical vorticity, horizontal winds overlaid with directional wind barbs, and potential temperature for the POL (left) and CLN (right) simulations at 100 minutes. [from Lerach et al. (2008).]

advancing gust front immediately south associated with the RFD and the FFD-based gust front to the north, both associated with confluent winds. The strongest near-surface winds exceed 45 m s^{-1} where the tangential winds due to vortex rotation coincide with the direction of supercell propagation. Unable to create a tornado, the CLN supercell produces a single, relatively straight gust front with confluent winds (maximum winds ~35 m s^{-1} behind the gust front) and alternating pockets of positive and negative vertical vorticity.

c. Microphysical effects on the cold pool

Ice and raindrop size distributions were compared between simulations to assess aerosol microphysical effects on precipitation. The POL case produced significantly more hailstones and small ice crystals, but of smaller

sizes as those in the CLN case. More ice was transported to the anvil in the POL supercell while more ice was available for precipitation processes in the CLN case. One might have expected the POL case to produce the strongest updrafts (via more latent heat release) and largest hailstones (Foote 1984). However, there were no significant differences in updraft strength (70 m s^{-1}) between simulations. The simulations neither produced major differences in raindrop sizes. However, raindrop concentrations varied significantly between simulations with respect to storm location. Fig. 6 displays 1-km rain concentrations and rain mixing ratios on Grid 2 at 90 min, overlaid with 30-dBZ model reflectivity boundaries at 1 km to present a relative sense of storm position. Maximum concentrations were similar between cases (CLN: 13000 vs. POL: 12000 m^{-3}). However, the highest concentrations in the POL supercell existed within the RFD while those of the CLN were in the FFD, as the RFD had nearly dissipated by this time. This translated to higher rain mixing ratios within the CLN FFD region.

The enhanced aerosol concentrations in the POL case resulted in a reduction in warm-rain processes producing numerous, small cloud droplets as compared to the CLN simulation. Larger amounts of supercooled drops were lofted in the updraft to act as embryos for ice formation, yielding many small ice particles that were eventually lofted into the storm's anvil.

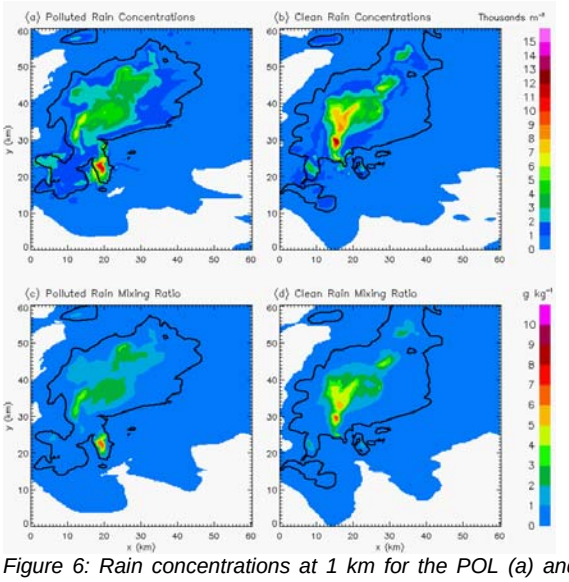

Figure 6: Rain concentrations at 1 km for the POL (a) and CLN (b) simulations (top panels) and rain mixing ratios at 1 km for the POL (c) and CLN (d) simulations (bottom panels) at 90 minutes on Grid 2. Plots are overlaid with 30-dBZ model reflectivity boundaries at 1 km.

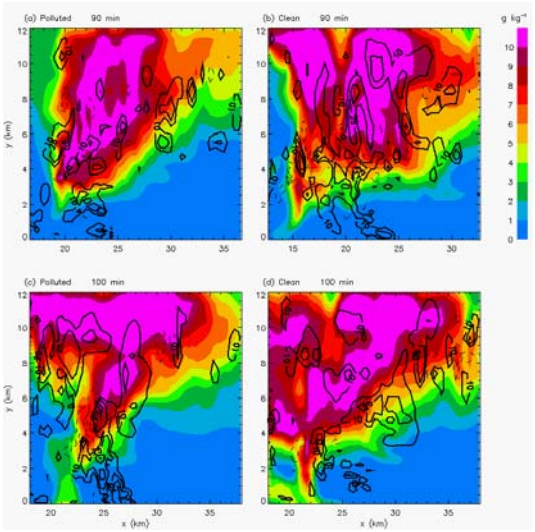

Figure 7: Constant 'y' vertical cross-sections of total mixing ratio overlaid with vertical vorticity (–25, -10, 10, 25, 50x10^{-3} s^{-1}) at 90 (top) and 100 minutes (bottom) on Grid 2 through the main updraft for the POL (left) and CLN (right) simulations. Cross-section regions are denoted in Fig. 1 as lines 'AB'.

The CLN supercell, which produced larger ice particles with greater terminal fall speeds, produced more ice used in cold-rain processes, leading to heavier precipitation rates in the CLN FFD compared to the POL case. The greater evaporative cooling rates associated with higher rainfall rates caused the FFD to surge out in the CLN simulation and destroy the RFD at the rear of the storm. Potential temperature at 24 m at the time of POL tornado vortex occurrence (Fig. 5g-h) shows that the minimum cold pool temperatures were similar between simulations. However, the POL cold pool remained approximately 2 K warmer near the developed vortex as compared to the CLN case, where the cold pool extended all the way to the storm's gust front. The stronger cold pool in the CLN storm hindered any vortex formation by advancing the gust front further away from the storm's core, thus locating the low-level updraft and vorticity source further away from the low-level mesocyclone compared to the POL case. While implied in Fig. 4, this is more evident in Fig. 7, which shows vertical cross-sections of vertical vorticity through the main updrafts of each simulation at 90 and 100 min. At 90 min, concentrated positive vertical vorticity greater than 25x10^{-3} s^{-1} was present within the low-level mesocyclone near 2 km as well as near the surface in both simulations. However, by 100 min the POL supercell exhibited a column of strong vertical vorticity extending from the low-level mesocyclone to the surface. The CLN

case failed to create such a column. The near-surface vertical vorticity at 90 min was located nearly 5 km further east from the vertical vorticity associated with the low-level mesocyclone in the CLN simulation.

4. Discussion

This study presented a preliminary look at possible effects of dust and pollutant aerosol acting as CCN and GCCN on supercell storms. Enhanced aerosol concentrations in the POL simulation reduced warm- and cold-rain processes within the RFD and FFD, resulting in lower precipitation rates. A relatively weak cold pool was produced at the updraft-downdraft interface due to low evaporative cooling rates, providing a favorable environment for tornadogenesis, where the low-level mesocyclone and near-surface vorticity provided by the RFD-based gust front remained vertically-stacked. This resulted in the formation of an EF-1 tornado while the CLN case failed to produce such a vortex. Heavier precipitation in the RFD and FFD in the CLN simulation produced more evaporative cooling, and thus a stronger surface cold pool that surged and destroyed the RFD structure. This resulted in a single gust front that advected away more rapidly from the storm system, separating the low-level vorticity source from the parent storm and thus hindering the tornadogenesis process. Studies such as Weisman and Klemp (1982) and Brooks et al. (1994) found similar potential failure mechanisms. The results were consistent with the findings of Markowski et al. (2002, 2003) and Snook and Xue (2008) regarding the importance of cold pool dynamics and the vertical alignment of vertical vorticity within a supercell to tornadogenesis. The key difference between the results of this study and Snook and Xue (2008) was the mechanism controlling evaporative cooling within downdrafts and thus cold pool strength (rain amount vs. rain and hail size, respectively). Nonetheless, this single, idealized study found that “other things being equal,” a polluted environment is more favorable for tornadogenesis. However, multiple factors control cold pool strength including surface fluxes of heat and water vapor (Ross et al. 2004), storm-relative midlevel flow (e.g., Brooks et al. 1994), convective available potential energy (CAPE; Markowski et al. 2002) and microphysics, particularly hail (van den Heever and Cotton 2004) and raindrop size (Gilmore et al. 2004). Furthermore, additional work is needed to address the robustness of the results presented.

Acknowledgments

Thanks to the late Ed Danielson, whose work in Project DUSTORM first suggested aerosols might influence tornadic thunderstorms (though his work on that subject remains unpublished), Louie Grasso of CIRA for his insight regarding this work, and Susan van den Heever of CSU, who supplied aerosol concentration profiles used in this study. This work was funded by National Science Foundation (NSF) Grant ATM-0638910.

References

Borys, R. D., D. H. Lowenthal, M. A. Wetzel, F. Herrera, A. Gonzalez, and J. Harris, 1998: Chemical and microphysical properties of marine stratiform cloud in the North Atlantic. *J. Geophys. Res*., **103**, 22073-22085.

Braham, R. R., Jr., R. G. Semonin, A. H. Auer, S. A. Changnon Jr., and J. M. Hales, 1981: Summary of urban effects on clouds and rain. METROMEX: A review and summary, *Meteor. Monogr.,* **40***,* Amer. Meteor. Soc., 141-152.

Brandes, E. A., 1978: Mesocyclone evolution and tornadogenesis: Some observations. *Mon. Wea. Rev.,* **106,** 995–1011.

Brooks, H. E., C. A. Doswell III, and R. B. Wilhelmson, 1994: The role of midtrospheric wind in the evolution and maintenance of low-level mesocyclones. *Mon. Wea. Rev.,* **122,** 126–136.

Burgess, D. W., R. A. Brown, L. R. Lemon, and C. R. Safford, 1977: Evolution of a tornadic thunderstorm. Preprints, *10th Conf. On Severe Local Storms,* Omaha, NE, Amer. Meteor. Soc., 84–89.

Clark, T. L., and R. D. Farley, 1984: Severe downslope windstorm calculations in two and three spatial dimensions using anelastic interactive grid nesting: A possible mechanism for gustiness. *J. Atmos. Sci.,* **41,** 329–350.

Cotton, W., R. A. Pielke Sr., R. L. Walko, G. E. Liston, C. J. Tremback, H. Jiang, R. L. McAnelly, J. Y. Harrington, M. E. Nicholls, G. G. Carrio, and J. P. McFadden, 2003: Rams 2001: Current status and future directions. *Meteor. Atmos. Phys*., **82**, 5-29.

Davies-Jones, R. P., 1982a: A new look at the vorticity equation with application to tornadogenesis. Preprints, *12th Conf. on Severe Local Storms,* San Antonio, TX, Amer. Meteor. Soc., 249–252.

Davies-Jones, R. P., 1982b: Observational and theoretical aspects of tornadogenesis. *Intense AtmosphericVortices,* L. Bengtsson and J. Lighthill, Eds., Springer-Verlag, 175–189.

Davies-Jones, R. P., 2000: Can the hook echo instigate tornadogenesis barotropically? Preprints, *20th Conf.on Severe Local Storms,* Orlando, FL, Amer. Meteor. Soc., 269–272.

Davies-Jones, R. P., and H. E. Brooks, 1993: Mesocyclogenesis from a theoretical perspective. *The Tornado: Its Structure, Dynamics, Prediction, and Hazards, Geophys. Monogr.,* **79**, Amer. Geophys. Union, 105–114.

Eagan, R. C., P. V. Hobbs, and L. F. Radke, 1974: Particle emissions from a large Kraft paper mill and their effects on the microphysical structure of warm clouds. J. Appl. Meteor., **13**, 535-552.

Eskridge, R. E., and P. Das, 1976: Effect of a precipitation-driven downdraft on a rotating wind field: A possible trigger mechanism for tornadoes? *J. Atmos. Sci.,* **33,** 70–84.

Foote, G. B., 1984: A study of hail growth utilizing observed storm conditions. *J. Climate Appl. Meteor*., **23**, 84-101.

Gaudet, B.J., and W.R. Cotton, 2006: Low-level mesocyclonic concentration by non-axisymmetric processes. Part I: Supercell and mesocyclone evolution. J. Atmos. Sci., 63, 1113-1133.

Gilmore, M. S., J. M. Straka, and E. N. Rasmussen, 2004: Precipitation uncertainty due to variations in precipitation particle parameters within a simple microphysics scheme. *Mon. Wea. Rev.*, **132,** 2610-2627.

Grasso, L. D., 2000: The dissipation of a left-moving cell in a severe storm environment. *Mon. Wea. Rev.,* **128,** 2797–2815.

Hobbs, P. V., L. F. Radke, and S. E. Shumway, 1970: Cloud condensation nuclei from industrial sources and their apparent influence on precipitation in Washington State. *J. Atmos. Sci.*, **27**, 81-89.

Kaufman, Y. J., and T. Nakajima, 1993: Effect of Amazon smoke on cloud microphysics and albedo: Analysis from satellite imagery. *J. Appl. Meteor.*, **32**, 729-744.

Lemon, L. R., 1974: Interaction of two convective scales within a severe thunderstorm: A case study. NOAA Tech. Memo. ERLNSSL, **71**, 43 pp. [NTIS COM-74-11642/AS.]

Lemon, L. R., and C. A. Doswell, 1979: Severe thunderstorm evolution and mesocyclone structure as related to tornadogenesis. *Mon. Wea. Rev.,* **107,** 1184–1197.

Lerach, D. G., B. J. Gaudet, and W. R. Cotton, 2008: Idealized simulations of aerosol influences on tornadogenesis. *Geophys. Res. Lett*., **35**, L23806, doi:10.1029/2008GL035617.

Leslie, L. M., and R. K. Smith, 1978: The effect of vertical stability on tornadogenesis. *J. Atmos. Sci.,* **35,** 1281–1288.

Ludlam, F. H., 1963: Severe local storms: A review. *Severe Local Storms, Meteor. Monogr.,* **27**, *Amer. Meteor. Soc*., 1–30.

Markowski, P.M., 2002: Hook echoes and rear-flank downdrafts: A review. *Mon. Wea. Rev.*, **130**, 852- 876.

Markowski, P. M., J. M. Straka, and E. N. Rasmussen, 2002: Direct surface thermodynamic observations within the rear-flank downdrafts of nontornadic and

tornadic supercells. *Mon. Wea. Rev.,* **130,** 1692– 1721.

Markowski, P. M., J. M. Straka, and E. N. Rasmussen, 2003: Tornadogenesis resulting from the transport of circulation by a downdraft: Idealized numerical simulations. *J. Atmos. Sci*., **60**, 795-823.

Nelson, S. P., 1977: Rear flank downdraft: A hailstorm intensification mechanism. Preprints, *10th Conf. on Severe Local Storms,* Omaha, NE, Amer. Meteor. Soc., 521–525.

Pielke, R. A., and Coauthors, 1992: A comprehensive meteorological modeling system -RAMS. *Meteor. Atmos. Phys*., **49**, 69-91.

Rosenfeld, D., 1999: TRMM observed first direct evidence of smoke from forest fires inhibiting rainfall. *Geophys. Res. Lett*., **26**, 3105-3108.

Rosenfeld, D., 2000: Suppression of rain and snow by urban and industrial air pollution. *Science*, **287**, 1793-1796.

Rosenfeld, D., R. Lahav, A. Khain, and M. Pinsky, 2002: The role of sea spray in cleansing air pollution over ocean via cloud processes. *Science*, **297**, 1667-1670.

Ross, A. N., A. M. Tompkins, and D. J. Parker, 2004: Simple models of the role of surface fluxes in convective cold pool evolution. *J. Atmos. Sci*., **61**, 1582-1595.

Rotunno, R., and J. B. Klemp, 1982: The influence of the shearinduced pressure gradient on thunderstorm motion. *Mon. Wea. Rev.,* **110,** 136–151.

Saleeby, S. M., and W. R. Cotton, 2004: A large droplet mode and prognostic number concentration of cloud droplets in the Colorado State University Regional Atmospheric Modeling System (RAMS). Part I: Module descriptions and supercell test simulations. *J. Appl. Meteor.*, 43, 182-195.

Seifert, A. and K. D. Beheng, 2006: A two-moment cloud microphysics parameterization for mixed-phase clouds. Part II: Maritime vs. continental deep convective storms, *Meteorol. and Atmos. Phys.*, **92**, 67-82.

Snook, N., and M. Xue, 2008: Effects of microphysical drop size distribution on tornadogenesis in supercell thunderstorms. *Geophys. Res. Lett.,* **35**, L24803, doi:10.1029/2008GL035866.

Trapp, R. J., and B. F. Fiedler, 1995: Tornado-like vortexgenesis in a simplified numerical model. *J. Atmos. Sci.,* **52,** 3757–3778.

van den Heever, S. C. and W. R. Cotton, 2004: The Impact of Hail Size on Simulated Supercell Storms. *J. Atmos. Sci.*, **61,** 1596-1609.

van den Heever, S. C., G. G. Carrio, W. R. Cotton, and P. J. DeMott, 2006: Impacts of nucleating aerosol on Florida storms. Part I: Mesoscale simulations. *J. Atmos. Sci*., **63**, 1752-1775.

Walko, R. L., 1993: Tornado spin-up beneath a convective cell: Required basic structure of the near-field boundary layer winds. *The Tornado: Its Structure, Dynamics, Prediction, and Hazards, Geophys. Monogr.,* **79**, Amer. Geophys. Union, 89–95.

Weisman, M. L., and H. W. Bluestein, 1985: Dynamics of numerically simulated LP storms. *Preprints, 14th Conf. On Severe Local Storms*, Indianapolis, IN, Amer. Meteor. Soc., 267-270.

Weisman, M. L., and J. B. Klemp, 1982: The dependence of numerically simulated convective storms on vertical wind shear and buoyancy. *Mon. Wea. Rev.,* **110,** 504–520.

Wicker, L. J., and R. B. Wilhelmson, 1995: Simulation and analysis of tornado development and decay within a three-dimensional supercell thunderstorm. *J. Atmos. Sci.,* **52,** 2675–2703.